Nanoscale

Accepted Manuscript

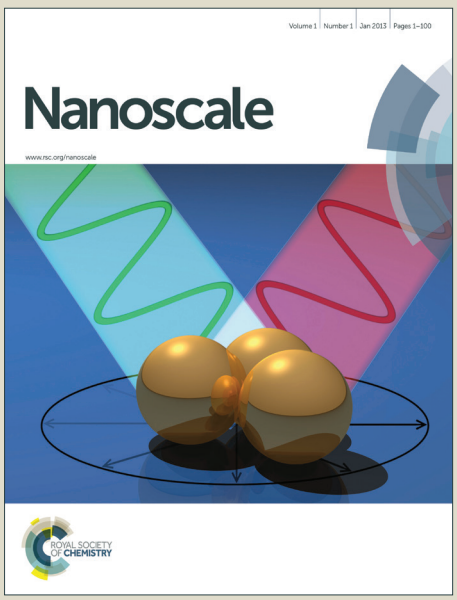

ROYAL SOCIETY OF CHEMISTRY

www.rsc.org/nanoscale

Nanoscale

RSCPublishing

PAPER

Preparation of $AgInS_2$ quantum dots/In_2S_3 co-sensitized photoelectrodes by a facile aqueous-phase synthesis route and their photovoltaic performance

Yuanqiang Wang[a,c], Qinghong Zhang[b], Yaogang Li[*b] and Hongzhi Wang[*a]

Cite this: DOI:

Received
Accepted

DOI:

www.rsc.org/nanoscale

In aqueous-phase system, $AgInS_2$ quantum dots (QDs) sensitized TiO_2 photoanodes were *in situ* prepared by the reaction of β-In_2S_3 nanocrystals and as-prepared TiO_2/Ag_2S-QDs electrodes, followed by a covering process with ZnS passivation layer. A facile successive ionic layer adsorption and reaction (SILAR) method was adopted to obtain TiO_2/Ag_2S-QDs electrodes. β-In_2S_3 nanocrystals synthesized by chemical bath deposition (CBD) process serve as the reactant of $AgInS_2$ as well as buffer layer between the interfaces of TiO_2 and $AgInS_2$ QDs. Polysulfide electrolyte and Pt-coated FTO glass count electrode were used to test photovoltaic performance of the constructed devices. The characteristics of the sensitized photoelectrodes were studied in more detail by electron microscopy, X-ray technique, optical and photoelectric performance measurements. $AgInS_2$ is the main photo-sensitizer for $TiO_2/AgInS_2$-QDs/In_2S_3 electrodes and excess In_2S_3 appears on the surface of the electrodes. Based on optimal Ag_2S SILAR cycle, the best photovoltaic performance of prepared $TiO_2/AgInS_2$-QDs/In_2S_3 electrode with short-circuit photocurrent density (J_{sc}) of 7.87 mA cm^{-2} and power conversion efficiency (η) of 0.70% under full one-sun illumination was achieved.

Introduction

Semiconductor quantum dots sensitized solar cells (QDSSCs) have recently drawn significant attention since inorganic quantum dots (QDs) with narrow band gap and appropriate band positions are considered to be next generation alternative sensitizers of costly dyes in dye-sensitized solar cells (DSSCs).[1-8] In comparison with those binary ones, multicomponent chalcogenide semiconductor nanomaterials, such as $CuInS_2$, $AgInS_2$ and related materials have attracted much attention in recent years for application in solar light energy conversion systems.[9-11] $AgInS_2$ can crystallize in both the chalcopyrite and orthorhombic phases exhibiting direct band gap of 1.87 and 1.98 eV, respectively,[12] which is suitable for the absorption of visible light. And it can form good matching heterojunction with Ag_2S,[13,14] Cu_2ZnSnS_4,[15] CdS,[16] or polymer matrix[17,18] due to its suitable lattice constant, making it a promising alternative for solar cell materials. Importantly, $AgInS_2$ is low-toxic as opposed to the cadmium chalcogenides.

As one of the most important I-III-VI materials, $AgInS_2$ was extensively studied on the electrical and optical properties. So far, most of the studies focus on the synthesis strategies of $AgInS_2$ nanocrystals (NCs) for biological application.[19-23] And several methods have been adopted to fabricate $AgInS_2$ thin films such as chemical spray pyrolysis,[24,25] physical vapor deposition,[26] and electrochemical deposition.[27] But these traditional preparation routes need harsh reaction conditions and the synthesized $AgInS_2$ films have poor crystal structure. Chemical bath deposition (CBD) and successive ionic layer adsorption and reaction (SILAR) routes were considered a convenient way to synthesize ternary sulphide thin films.[28,29] Very recently, the $AgInS_2$ NCs[17] and Cu-doped $AgInS_2$[18] NCs have been incorporated in organic-inorganic hybride optoelectronic devices. Very poor total energy conversion efficiency is obtained for solar cells made using organic capped $AgInS_2$ NCs because the insulating organic ligands inhibit electron injection to core NCs.[30] It should be noted that ITO/ZnO/ZnS/$AgInS_2$/P3HT/Pt hybrid solar cells showed a

[a] *State Key Laboratory for Modification of Chemical Fibers and Polymer Materials, College of Materials Science and Engineering, Donghua University, Shanghai 201620, People's Republic of China. E-mail: wanghz@dhu.edu.cn ; Tel: +86-21-67792881; fax: +86-21-67792855*

[b] *Engineering Research Center of Advanced Glasses Manufacturing Technology, Donghua University, Shanghai 201620, People's Republic of China. E-mail: yaogang_li@dhu.edu.cn*

[c] *College of Chemistry and Chemical Engineering, Shanghai University of Engineering Science, Shanghai 201620, People's Republic of China.*

† Electronic supplementary information (ESI) available: Photograph images, FESEM images, Optical absorption spectra, Photocurrent voltage characteristics of the photoelectrodes obtained by CBD of In_2S_3 and *in situ* reaction with different cycle of Ag_2S SILAR deposition on TiO_2 films. See DOI:

power conversion efficiency (PCE) of 2.11%, which is the relatively highest value ever reported for ZnO-based all-solid-state hybrid solar cells. [31]

Up to now, there are only few reports about $AgInS_2$ NCs sensitized solar cells. Nag *et al*. prepared $AgInS_2$ NCs by a post-synthesis annealing of NC dispersion that modifies the size and defect density of the NCs, and solution processed $AgInS_2$ NCs were used to form the photoanode of the QDSSCs exhibiting the PCE of 0.8% and short-circuit current density of 4.62 mA cm^{-2}.[32] Torimoto *et al*. reported sandwich-type solar cells fabricated with the ZnS-$AgInS_2$-loaded ZnO nanorod electrode as a working electrode and an acetonitrile solution containing the redox couple of I^-/I_3^- exhibited a photoresponse in the visble light region.[33] It has been reported in the literatures that the high conversion efficiency of ternary chalcogenides QDSSCs is generally caused by interfacial charge-transfer processes at TiO_2 film and QDs sensitizer.[34,35] Approaches such as decreasing the charge recombination within the QDSSCs by modifying the blocking layer,[36] doping of CdS QDs with Mn^{2+} to improve the lifetime of trapped electron,[37] the deposition of Ru-dyes and QDs as hybrid photosensitizers, [38] and a buffer layer[39] has been carried out. Applying a buffer layer such as In_2S_3 between TiO_2 and $CuInS_2$ can suppress the interface electron recombination so that improve the cell performance.[40,41] In_2S_3, a typical III-VI group sulphide, exists in three different structure forms: α-In_2S_3 (defect cubic structure), β-In_2S_3 (defect spinel structure) and γ-In_2S_3 (layered hexagonal structure). In fact, β-In_2S_3 is a well n-type photoactive semiconductor with a direct band gap about 2.0 eV, a relative large exciton Bohr radius approximately 34 nm and a high carrier mobility.[42,43] To further improve the performance of chalcogenide-based solar cells, an intermediate band gap layer can be incorporated in a CIS solar cell to increase its photoelectric performance.[35] For this purpose, $AgInS_2$ QDSSCs embedded β-In_2S_3 layers should be developed.

Herein, for the first time, we fabricate $AgInS_2$-QDs/In_2S_3 co-sensitized solar cells by a facile aqueous-phase synthesis route. The growth process of $AgInS_2$-QDs/In_2S_3 on TiO_2 film was demonstrated in detail. By using the Pt counter electrode (CE) and polysulfide electrolyte to assemble a QDSSC, the $AgInS_2$-QDs/In_2S_3 co-sensitizers provide the PCE of 0.70% and the short-circuit current density of 7.87 mA cm^{-2} under one-sun illumination.

Experimental section

Materials

Silver(I) acetate (Ag(OAc), 99+%), sodium sulfide ($Na_2S{\cdot}9H_2O$, 98+%), indium chloride ($InCl_3{\cdot}4H_2O$, 98+%), thioacetamide (CH_3CSNH_2, 98+%), citric acid ($C_6H_8O_7{\cdot}H_2O$, 98+%), ethanol (99.5%), zinc acetate ($Zn(OAc)_2{\cdot}2H_2O$, 99+%), sulfur (S, 99.5%), potassium chloride (KCl, 99.5%) were purchased from Sinopharm Chemical Reagent Co. (Shanghai, China). TiO_2 powder (P25, a mixed phase of 70% anatase and 30% rutile; average size 25nm+) from Degussa (Japan) was used to prepare TiO_2 anatase nanoparticles for photoelectrodes. Ethylcellulose and terpineol from Fluka (Germany) were used to suspend TiO_2 particles in viscous solutions. All the materials were used without further purification. Fluorine-doped tin oxide (FTO) conducting glass substrate (2.3 mm thick, 14 Ω/□) was purchased from Nippon Sheet Glass.

Preparation of TiO_2/Ag_2S-QDs electrodes

Mesoporous TiO_2 electrodes were prepared by following a method reported earlier.[44, 45] In brief, FTO glass was cleaned in a detergent solution using an ultrasonic bath for 15 min, and then rinsed with water and ethanol. Two layers of TiO_2 were deposited on FTO, a blocking layer and active layer. The blocking layer was deposited by treating the glass in a 40 mM $TiCl_4$ aqueous solution at 70 °C for 30 min followed by annealing at 500°C for 30 min. The active TiO_2 layer (P25 paste) was coated on top of the blocking layer by the doctor blade technique. The film was dried at 125 °C for 6 min followed by annealing 500 °C for another 30 min. A post treatment process of the calcined film was similar with that of blocking layer. The thickness of the TiO_2 mesoporous electrode was approximately 9 μm, measured by an optical profiler (Wyko NT9100, Veeco Co., USA). TiO_2/Ag_2S-QDs electrodes were subsequently prepared by SILAR method.[46] The electrode was dipped into 0.02 M Ag(OAc) aqueous solution for 30 s, rinsing with water, subsequent 30 s immersion in 0.05 M Na_2S aqueous solution followed by further rinsing with water. Each series of two immersions was considered as one SILAR cycle.

Fabrication of the $AgInS_2$-QDs/In_2S_3/ZnS QDSSCs

QDs-sensitized solar cells consisting of $AgInS_2$ QDs sensitizer with In_2S_3 buffer layer were prepared by CBD of In_2S_3 and in situ reaction with TiO_2/Ag_2S-QDs films with one-step method. A precursor aqueous solution of In_2S_3 was prepared from a mixture of $InCl_3$ (0.01 M), CH_3CSNH_2 (0.04 M). During the mixing procedure, $C_6H_8O_7$ (0.06 M) was added with the chemical solution for the formation of indium complexe. The resulting clear mixture was transferred into a 70 mL Teflon-lined stainless steel autoclave, holding a vertically oriented FTO glass substrate (with a Ag_2S/TiO_2 film), which was then sealed and maintained at 150 °C for 3 h. The substrate was then rinsed with water and ethanol and dried at room temperature. The electrode was marked as TiO_2/$AgInS_2$(n)-QDs/In_2S_3 according to the different Ag_2S SILAR cycle (where n is Ag_2S SILAR cycle). All the electrodes analyzed in this study have been coated with ZnS, carried out by two SILAR cycle consisting of twice dipping alternatively in the 0.1 M $Zn(OAc)_2$ and 0.1 M Na_2S aqueous solution for 1 min per dip. The QDSSC was sealed in a sandwich structure with a spacer film (50 μm thick polyester film, DuPont) by using Pt-coated FTO glass. The space between the electrodes was filled with the polysulfide electrolyte which consisted of Na_2S (2 M), S (2 M), and KCl (0.2 M), using pure water as solvent. A mask with a window of 0.25 cm^2 was clipped on the photoanode side to define the active area of the cell.

Characterization

High-resolution transmission electron microscopy (HRTEM) images were obtained using a JEM 2100 F(JEOL Co., Japan) operating at 200 kV. The surface morphology and structure of the resulting films was studied using a field emission scanning electron microscope (FESEM, S-4800, Hitachi, Japan). The crystal structure was investigated by an X-ray diffraction technique (XRD, D/max 2550 V, Rigaku, Japan) with Cu Kα (λ = 0.154 nm) radiation at 40 kV and 200 mA in 2θ ranging from 20° to 80°. X-ray photoelectron spectra (XPS) were recorded on an ESCALab MKII X-ray photoelectron spectrometer. UV-visible absorption spectra were recorded using a spectrophotometer (Lambda 950, Perkin-Elmer Co., USA). Photocurrent-voltage characteristics (J–V curves) of QDSSCs were measured using a Keithley 2400 Source Meter under

illumination of simulated sunlight (100 mW cm^{-2}) provided by a Newport solar simulator (Model 96160) with an AM 1.5G filter. Incident photon-to-current conversion efficiency (IPCE) spectra were measured as a function of wavelength from 350 to 800 nm using a specially designed IPCE system (Newport, USA) for the QDSSCs.

Results and discussion

In aqueous-phase system, $AgInS_2$-QDs sensitized TiO_2 photoanodes were *in situ* prepared by the reaction of β-In_2S_3 nanocrystals and as-prepared TiO_2/Ag_2S-QDs electrodes. TiO_2/Ag_2S-QDs electrodes were obtained by a facile successive ionic layer adsorption and reaction (SILAR) method. β-In_2S_3 nanocrystals synthesized by chemical bath deposition (CBD) process serve as the reactant of $AgInS_2$ as well as buffer layer between the interfaces of TiO_2 and $AgInS_2$ QDs. The overall reactions are presented as the follow:

$$Ag^+ + S^{2-} \rightarrow Ag_2S \quad (1)$$

(The reaction was processed on TiO_2 films)

$$L \rightleftarrows L^- + H^+ (L \text{ is citric acid}) \quad (2)$$

$$In^{3+} + L^- \rightleftarrows InL_3 \quad (3)$$

$$CH_3CSNH_2 + H^+ \rightarrow CH_3CNH^+ + H_2S \quad (4)$$

$$H_2S \rightleftarrows HS^- + H^+ \rightleftarrows S^{2-} + 2H^+ \quad (5)$$

$$In^{3+} + S^{2-} \rightarrow In_2S_3 \quad (6)$$

$$Ag_2S + In_2S_3 \rightarrow 2AgInS_2 \quad (7)$$

The high-resolution TEM (HRTEM) image of the $TiO_2/AgInS_2$-QDs/In_2S_3 composite in Fig. 1 clearly depicts the crystalline lattice fringes of the involved species. The lattice spacing distance of 0.352 nm, illustrated in the right zone of the image, corresponds to the (101) plane of anatase TiO_2. The lattices with spacing distances of 0.334 and 0.325 nm round TiO_2 particle encompassed by red lines correspond to the (112) plane of the tetragonal $AgInS_2$ (JCPDS file no. 75-0117) and (311) plane of the In_2S_3 (JCPDS file no. 84-1385), respectively. The In_2S_3 coating with CBD method is in close contact with both the $AgInS_2$ QDs and TiO_2 particles.

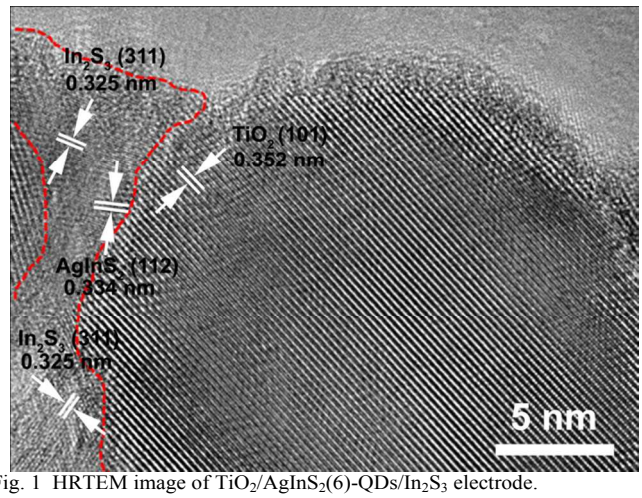

Fig. 1 HRTEM image of $TiO_2/AgInS_2$(6)-QDs/In_2S_3 electrode.

Fig. 2 shows a series of color changes for the TiO_2 electrodes after sensitization in the reaction process. TiO_2/In_2S_3 electrode was prepared as a reference. The TiO_2 film was originally white and semi-transparent, becoming black-brown when it was coated with Ag_2S QDs and red-brown when it coated with $AgInS_2$-QDs/In_2S_3. Due to the quantum confinement effect in the optics, the color for the $TiO_2/AgInS_2$-QDs/In_2S_3 electrode is distinct with black bulk $AgInS_2$. It was also found that the color of $TiO_2/AgInS_2$-QDs/In_2S_3 electrode changes from pale red-brown to dark reddish brown, indicating the increase of $AgInS_2$-QDs layer thickness (see Fig. 1S†). The present claybank color on $TiO_2/AgInS_2$-QDs/In_2S_3 electrodes indicates the deposition of In_2S_3 films on the bare FTO glass.

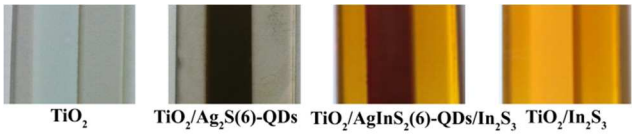

Fig. 2 The photograph images of the corresponding electrodes.

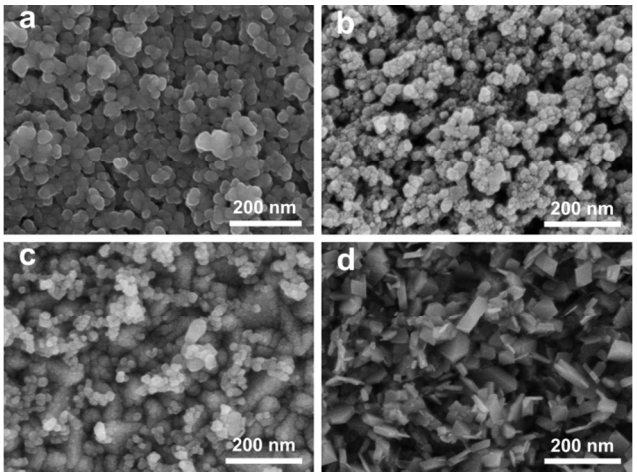

Fig. 3 (a) FESEM images (top view) of (a) plain TiO_2 film, (b) TiO_2/Ag_2S-QDs electrode prepared by 6 cycles of Ag_2S SILAR deposition, (c) TiO_2/In_2S_3 electrode prepared by In_2S_3 CBD deposition and (d) $TiO_2/AgInS_2$(6)-QDs/In_2S_3 electrode.

FESEM images in Fig. 3 demonstrate the surface topography of the electrodes at different reaction stages. SILAR method was used to deposit Ag_2S on TiO_2 films as the basic electrode, and the growth mechanism of the Ag_2S-QDs on the TiO_2 films was monitored with FESEM image (see Fig. 3a, b). It is clear that the entire surface of the FTO substrate is covered uniformly and densely with TiO_2 nanoparticles from Fig. 3a. The average particle diameter is approximate 30 nm and the average pore size among TiO_2 nanoparticles is less than 10 nm. After assembled with Ag_2S for 6 cycles, the TiO_2 nanoparticles structure is retained, and the Ag_2S particles could be generated in the pores as well as on the surface of porous TiO_2 films as shown in Fig. 3b. In addition, the small diameter of pores of the TiO_2 films restricts further growth of the Ag_2S particles. Thus, Ag_2S particles were smaller in the porous TiO_2 films, meaning that the size of Ag_2S is in the scope of quantum dot. Fig. 3c shows the surface topography of TiO_2/In_2S_3 film prepared by CBD method as comparison. The surface of the as-deposited film shows a uniform granular structure with very-well-defined grain boundaries and with some larger grains dispersed on the film surface. The grains have an irregular round shape. Fig. 3d shows the surface morphology of $AgInS_2$(6)-QDs/In_2S_3 co-sensitized TiO_2 electrode. It was found that $AgInS_2$ nanoparticles with pyramid-like shape appear on the surface of the film. The surface morphology of $TiO_2/AgInS_2$-QDs/In_2S_3 films prepared with different Ag_2S SILAR cycle seem to be slightly affected by the Ag_2S SILAR cycles (see Fig. 2S†). All the samples show the similar surface morphology, however, as

the Ag_2S SILAR cycle increases, the pyramid-like structure becomes denser and the size of $AgInS_2$ particles become larger on the surface of electrode.

The valence states and composition of the surface of $TiO_2/AgInS_2(6)$-QDs/In_2S_3 electrode were further investigated by XPS (see Fig. 4).

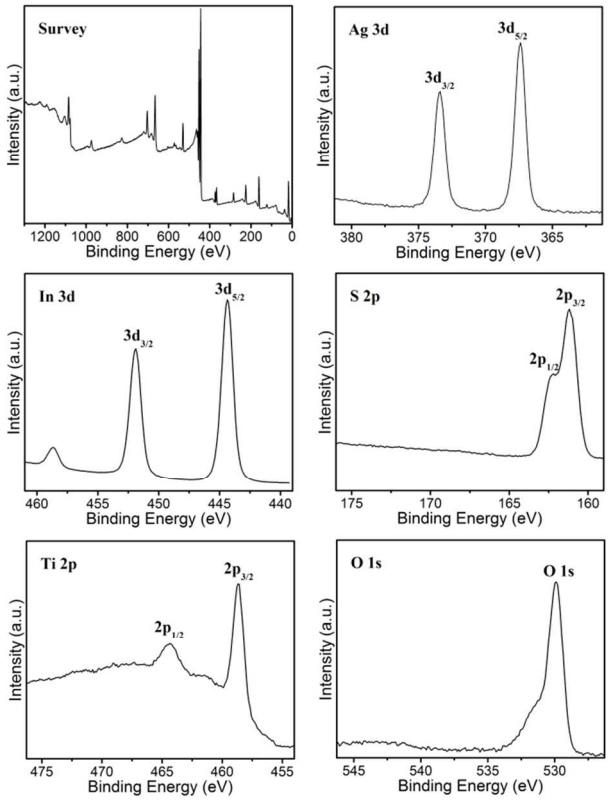

Fig. 4 XPS survey, Ag 3d, In 3d, S 2p, Ti 2p and O 1s of the surface of $TiO_2/AgInS_2(6)$-QDs/In_2S_3 electrode.

Table 1 The elementary composition of calculated from XPS spectrum of the surface of $TiO_2/AgInS_2(6)$-QDs/In_2S_3 electrode.

Name	Peak Binging Energy (eV)	FWHM (eV)	Atomic (%)
Ag3d	367.4	0.94	2.3
In3d	444.4	1.1	22.41
S2p	161.2	1.12	27.81
Ti2p	458.5	1.09	29.48
O1s	529.9	1.31	17.99

The Ag 3d, In 3d, S2p, Ti2p and O1s were examined, respectively, which confirm the presence of these elements in the typical sample. The binding energies of Ag $3d_{3/2}$ and Ag $3d_{5/2}$ for $AgInS_2$ were located at 373.5 eV and 367.4 eV with a peak splitting of 6 eV, which is consistent with the standard reference XPS of Ag^+. The In 3d peaks were located at 444.4 eV and 451.9 eV with a peak splitting of 7.5 eV, matching well with In^{3+}. The S 2p peaks splitting of 161.2 eV and 162.3 eV with a peak splitting of 1.1 eV, which corresponds to a binding energy of S^{2-}.[47] The Ti 2p spectra exhibits two peaks corresponding to the binding energies of 458.5 eV (Ti $2p_{3/2}$) and 464.2 eV (Ti $2p_{1/2}$), resulting from the Ti of TiO_2. The binding energies of O 1s were located into two peaks, the peak at 529.9 eV, resulting from the crystal lattice oxygen of TiO_2 and the peak at 532 eV, corresponding to the hydroxyl oxygen. It can be seen in Table 1 through the quantification of peaks, there are excess In, S elements according to the stoichiometric coefficient of $AgInS_2$, showing the sensitizers consist of $AgInS_2$ and In_2S_3 over the electrode. And there are excess O elements according to the stoichiometric coefficient of TiO_2 attributing to the hydroxyl oxygen on the surface of the sample.

To explore the formation process of $AgInS_2$-QDs/In_2S_3 co-sensitized electrodes, the TiO_2 electrodes after sensitization at different reaction stages were monitored by XRD analyses in Fig. 5. There are unconspicuous Ag_2S diffraction peaks according to the similar XRD patterns of $TiO_2/Ag_2S(6)$ electrode and TiO_2 electrode, showing the size of Ag_2S is in quantum dot range. In addition, it is also not easy to determine $AgInS_2$ phase (JCPDS file no. 75-0117) over $AgInS_2(6)$-QDs/In_2S_3 co-sensitized TiO_2 electrode due to smaller size of $AgInS_2$ QDs and the higher intensity of the TiO_2 (P25) diffraction peak. However, the main diffraction peaks such as (111), (400) and (511) diffraction peaks of β -In_2S_3 (JCPDS file no. 84-1385) appear on the XRD pattern of $AgInS_2$-QDs(6)/In_2S_3 co-sensitized electrode, indicating that there are excess β -In_2S_3 over the electrode.

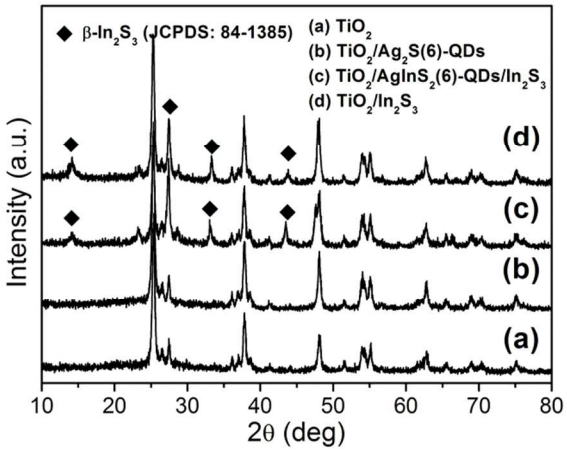

Fig. 5 XRD patterns of plain TiO_2 film, $TiO_2/Ag_2S(6)$-QDs electrode prepared by 6 cycles of Ag_2S SILAR deposition, TiO_2/In_2S_3 electrode prepared by In_2S_3 CBD deposition and $TiO_2/AgInS_2(6)$-QDs/In_2S_3 electrode.

UV-vis absorption spectroscopy was used to track the formation of $AgInS_2$-QDs/In_2S_3 co-sensitized electrodes and investigate the suitability for photovoltaic application. Fig. 6 shows the absorption spectra of the correlative electrodes during the preparation process of $TiO_2/AgInS_2$-QDs/In_2S_3 photoanode that from the plain TiO_2, TiO_2/Ag_2S-QDs to $TiO_2/AgInS_2$-QDs/In_2S_3 electrode. TiO_2/In_2S_3 electrode was chosen as a comparison. The spectrum shows that the plain TiO_2 can mainly absorb UV light with wavelength smaller than 420 nm. The TiO_2/Ag_2S-QDs electrode can absorb UV to near-infrared light, but its optical absorption ability is rather weak, probably being bad for solar cell performance. The TiO_2 film with In_2S_3 CBD deposition, the light absorbance of the electrode was enhanced in the visible region, and its absorption band edge is about 530 nm. The prepared $TiO_2/AgInS_2$-QDs/In_2S_3 electrode has excellent optical absorption performance not only UV region, but also in the visible region. A shoulder appears between 530 and 600 nm with a long tail

extending to longer wavelengths, which is mainly due to the formation of the $AgInS_2$ layer coated on the TiO_2 electrode. These results confirm that $AgInS_2$ layer can effectively improve the light absorption property of TiO_2 film. It was also found that the absorption spectra of the $TiO_2/AgInS_2$-QDs/In_2S_3 electrodes obtained by CBD of In_2S_3 and *in situ* reaction with different cycles of Ag_2S SILAR deposition on TiO_2 film are similar (see Fig. 3S†). The absorption spectra of the prepared $TiO_2/AgInS_2$-QDs/In_2S_3 electrodes were red-shifted with the increase of the Ag_2S SILAR cycles probably because of the increase of $AgInS_2$-QDs size or the increase of $AgInS_2$-QDs layer thickness. The enhanced absorption in the longer wavelength region is probably due to the remission of quantum confinement effect on the $AgInS_2$ QDs.

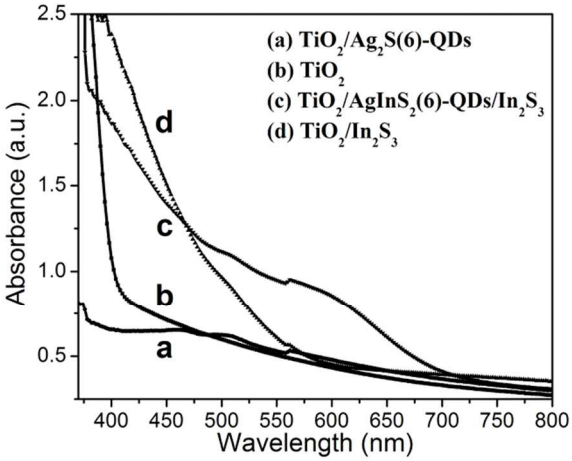

Fig. 6 Optical absorption spectra of the plain TiO_2 film, TiO_2/Ag_2S-QDs electrode prepared by 6 cycles of Ag_2S SILAR deposition, $TiO_2/AgInS_2$(6)-QDs/In_2S_3 electrode and TiO_2/In_2S_3 electrode prepared by CBD of In_2S_3 for 3 h on the plain TiO_2 film.

We fabricated QDSSCs using the FTO/$TiO_2/AgInS_2$-QDs/In_2S_3/ZnS as the photoanode and a Pt electrode as the cathode along with a polysulfide electrolyte between the electrodes. Fig. 7 shows schematic descriptions of the working principle of a QDSSC and its charge transfer mechanism, respectively. β-In_2S_3 QDs obtained by CBD method react with as-prepared Ag_2S QDs in the holes of TiO_2 films to form $AgInS_2$@In_2S_3 QDs and there are also excess $AgInS_2$ and In_2S_3 particles on the surface of the electrodes. $AgInS_2$ QDs absorb photons and generate electron-hole pairs. These photo-generated electrons can be efficiently transferred from $AgInS_2$ QDs to the mesoporous TiO_2 layer, finally collected by the FTO glass contact. Moreover, there are non-radial recombination electron and hole *via* the defect state as marked in Fig. 7(b) with a green dotted arrow.[32] At the same time, the photo-generated holes are scavenged by the polysulfide based redox electrolyte. $AgInS_2$-QDS/In_2S_3 surface was passivated with a wider band gap semiconductor (ZnS, 3.6 eV)[48] to prevent the leakage of current from $AgInS_2$-QDS/In_2S_3 to the electrolyte.

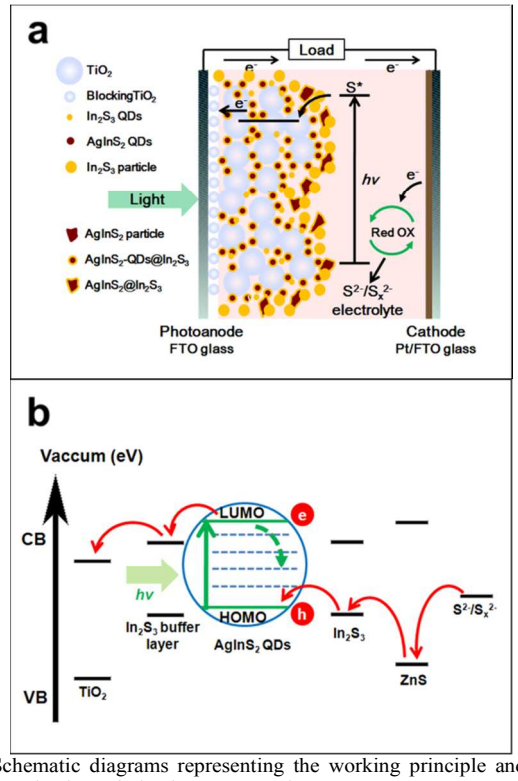

Fig. 7 Schematic diagrams representing the working principle and charge transfer mechanism of $TiO_2/AgInS_2$-QDs/In_2S_3 QDSSC.

Fig. 8 presents the photocurrent-voltage characteristics (*J-V* curves) of the $TiO_2/AgInS_2$-QDs(6)/In_2S_3 co-sensitized photonaode with Pt counter electrode and polysulfide electrolyte. TiO_2/In_2S_3 electrode prepared by CBD of In_2S_3 on TiO_2 film for 3 h and TiO_2/Ag_2S(6)-QDs electrode prepared by SILAR method were used as comparison. The intermediate values for the main resultant photovoltaic parameters based on five parallel cell devices and the error intervals of PCE (η) are summarized in Table 2. For the cell based on just Ag_2S(6)-QDs or In_2S_3 sensitized TiO_2 photo-electrode, a short-circuit photocurrent density (J_{sc}) of 0.49 or 1.19, an open-circuit photovoltage (V_{oc}) of 0.19 or 0.23 V, a fill factor (*FF*) of 0.34 or 0.31 and a PCE (η) of 0.03 or 0.08 were revealed respectively. The poor photovoltaic performance may be attributed to the poor light absorption ability or the unmatched energy level. For $AgInS_2$(6)-QDs/In_2S_3 co-sensitized QDSSC, the *J-V* curve reveals that J_{sc}=7.87 mA cm^{-2}, V_{oc}=0.32 V, and η=0.70%, which are higher than those of TiO_2/Ag_2S(6)-QDs and TiO_2/In_2S_3 electrodes. The higher photocurrent density and efficiency is probably because of the broader light absorption spectrum and the better charge carriers generation ability of $AgInS_2$ QDs for $AgInS_2$(6)-QDs/In_2S_3 co-sensitized TiO_2 photo-electrode. In general, the current density for QDSSCs are determined by the initial number of photo-generated charge carriers, the electron injection efficiency from QD-sensitizers to photo-electrodes, and the recombination rate between the injected electrons and holes of excited QDs or redox species in the electrolyte. The IPCE is defined as the number of photo-generated charge carriers contributing to the current per incident photon. Fig. 9 compares the IPCE spectra of the QDSSCs. The IPCE spectra of the QDSSCs were basically consistent with the corresponding UV-Vis spectra shown in Fig.6. $TiO_2/AgInS_2$-QDs(6)/In_2S_3 QDSSC shows a maximum IPCE of about 37% from 500 to 625 nm, which is much higher than that of TiO_2/In_2S_3 and TiO_2/Ag_2S(6)-QDs electrodes.

Therefore, we believe that $AgInS_2$-QDs are the main photo-sensitizers. On the other hand, the lower *FF* indicates the increasing of carrier recombination on the interfaces between TiO_2 and QDs sensitizer or electrolyte and CE. It is well known that Pt is not a good catalyst for polysulfide regeneration, which leads to poor fill factors for QDSSCs because their surface activity and conductivity are suppressed as result of adsorption of the sulfur atom. [49] The lower open-circuit photovoltage of $TiO_2/AgInS_2$-QDs(6)/In_2S_3 QDSSC may be due to the surface defects of the synthesized $AgInS_2$ QDs. β -In_2S_3 serves not only as the reactant of $AgInS_2$ but also intermediate band gap layer that may change the unmatched band alignments in the heterostructure between TiO_2 and $AgInS_2$ QDs. However, the excess β -In_2S_3 particles on the surface of $TiO_2/AgInS_2$-QDs/In_2S_3 co-sensitized photonaodes lead to unhomogeneous In_2S_3 deposition, which may affect the surface state of the $AgInS_2$ QDs.

In addition, based on the same construction for the given $TiO_2/AgInS_2$-QDs/In_2S_3 QDSSCs system, it is reasonable that the photocurrent density and energy conversion efficiency are directly affected by the initial Ag_2S SILAR cycles (See Fig. 4S† and Table 1 S†). With increasing the Ag_2S SILAR deposition from 2 cycles to 6 cycles, the J_{sc} of $TiO_2/AgInS_2$-QDs/In_2S_3 photoanodes increases substantially from 3.39 to 7.87 mA cm^{-2}. The increase of J_{sc} is attributed to extending the light absorption range and the increase in absorption ability with red-shift of the absorption onset of $AgInS_2$-QDs/In_2S_3 sensitizer. The increase of incorporated amount of $AgInS_2$-QDs can not only contribute to absorb more photons to generate more photoexcited electrons, but also form a uniform and dense shell to reduce direct contact areas between the bare TiO_2 surface and polysulfide electrolyte.[50, 51] However, the J_{sc} and η were found to decrease when the Ag_2S coating increased to 8 cycles. The possible reason for the reduced cell performance may be attributed to the aggregations and growth of the Ag_2S QDs (See Fig. 2S†), which will result in the presence of subsequently synthesized $AgInS_2$ QDs with no direct contact with the TiO_2, leading to block the infiltration of the electrolyte into the photoelectrode, thereby decreasing the regeneration efficiency of the solar cell.[52, 53]

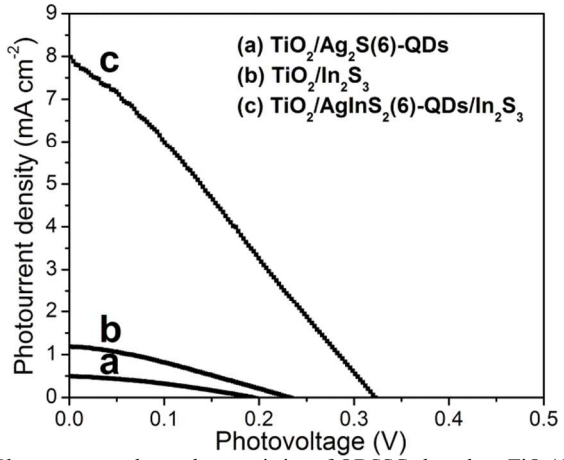

Fig. 8 Photocurrent voltage characteristics of QDSSCs based on TiO_2/Ag_2S (SILAR for 6 cycles), TiO_2/In_2S_3 (CBD for 3h), $TiO_2/AgInS_2$(6)-QDs/In_2S_3 electrodes.

Table 2 Photovoltaic parameters of QDSSCs based on TiO_2/Ag_2S (SILAR for 6 cycles), TiO_2/In_2S_3 (CBD for 3h), $TiO_2/AgInS_2$(6)-QDs/In_2S_3 electrodes.

Photoanode	J_{sc} (mA cm^{-2})	V_{oc} (V)	*FF*	η (%)
TiO_2/Ag_2S-QDs(6)	0.49	0.19	0.34	0.03±0.01
TiO_2/In_2S_3	1.19	0.23	0.31	0.08±0.01
$TiO_2/AgInS_2$(6)-QDs/In_2S_3	7.87	0.32	0.28	0.70 ± 0.02

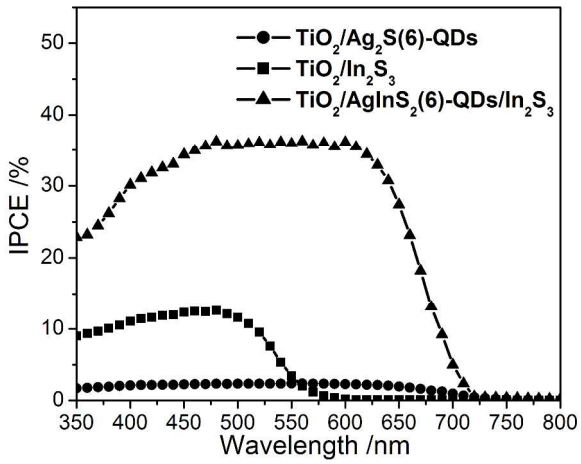

Fig. 9 IPCE spectra of QDSSCs based on TiO_2/Ag_2S (SILAR for 6 cycles), TiO_2/In_2S_3 (CBD for 3h), $TiO_2/AgInS_2$(6)-QDs/In_2S_3 electrodes.

Conclusions

As one of the most important I-III-VI materials, $AgInS_2$ was extensively studied on the electrical and optical properties，and the reports about $AgInS_2$ QDs sensitized solar cells are quite few. In this study, for the first time, we have presented a facile aqueous-phase synthesis route to prepared QDs-sensitized photoelectrodes consisting of $AgInS_2$-QD/In_2S_3 co-sensitizers based on CBD of In_2S_3 and *in situ* reaction with TiO_2/Ag_2S-QDs films obtained by SILAR method. $AgInS_2$-QDs are the main photo-sensitizers. $AgInS_2$ nanoparticles with pyramid-like shape and excess In_2S_3 layer were found on the surface of the $TiO_2/AgInS_2$-QDs/In_2S_3 electrodes. The $TiO_2/AgInS_2$(6)-QDs/In_2S_3 QDSSC shows the better photovoltaic performance with J_{sc} of 7.87 mA cm^{-2}, η of 0.70% and maximum IPCE of about 37% than those of the TiO_2/Ag_2S(6)-QDs and TiO_2/In_2S_3 QDSSCs attributing to the broader light absorption spectrum and the better charge carriers generation ability of $AgInS_2$ QDs for $AgInS_2$(6)-QDs/In_2S_3 co-sensitized TiO_2 photo-electrode. The absorption spectra of the prepared $TiO_2/AgInS_2$-QDs/In_2S_3 electrodes were red-shifted with the increase of the Ag_2S SILAR cycles probably because of the increase of $AgInS_2$-QDs size or the increase of $AgInS_2$-QDs layer thickness. Based on the same construction for the given $TiO_2/AgInS_2$-QDs/In_2S_3QDSSCs system, the photocurrent density and energy conversion efficiency are directly affected by the initial Ag_2S SILAR cycles. We expect that this facile synthesis method should provide an insight into the fabrication of heterojunction thin film solar cells based on multicomponent chalcogenide.

Acknowledgements

We gratefully acknowledge the financial support by Natural Science Foundation of China (No.51172042), Specialized Research Fund for the Doctoral Program of Higher Education (20110075130001), Science and Technology Commission of Shanghai Municipality (12nm0503900, 13JC1400200, 15ZR1401200), Innovative Research Team in University (IRT1221) and the Program of Introducing Talents of Discipline to Universities (No.111-2-04).

Notes and references

1 R. B. David and V. K. Prashant, *Adv. Funct. Mater.*, 2009, **19**, 805.
2 W. T. Sun, Y. Yu, H. Y. Pan, X. F. Gao, Q. Chen and L. M. Peng, *J. Am. Chem. Soc.*, 2008, **130**, 1124.
3 J. H. Bang and P. V. Kamat, *Adv. Funct. Mater.*, 2010, **20**, 1970.
4 X. N. Wang, H. J. Zhu, Y. M. Xu, H. Wang, Y. Tao, S. Hark, X. D. Xiao and Q. A. Li, *ACS Nano*, 2010, **4**, 3302.
5 K. Santhosh and A. Samanta, *J. Phys. Chem. C*, 2012, **116**, 20643.
6 J. B. Sambur, T. Novet and B.Parkinson, *Science*, 2010, **330**, 63.
7 H. J. Lee, Henry C. Leventis, S. J.Moon, P. Chen, S. Ito, Saif A. Haque, T. Torres, F. Nüesch, T. Geiger, Shaik M. Zakeeruddin, M. Grätzel and M. K. Nazeeruddin, *Adv. Funct. Mater.*, 2009, **19**, 2735.
8 P. R. Yu, K. Zhu, Aderew G. Norman, S. Ferrere, A. J. Frank and Arthur J. Nozik, *J. Phys. Chem. B*, 2006, **110**, 25451.
9 I. Tsuji, H. Kato, H. Kobayashi and A. Kudo, *J. Am. Chem. Soc.*, 2004, **126**, 13406.
10 I. Tsuji, H. Kato and A. Kudu, *Chem. Mater.*, 2006, **18**, 1969.
11 G. P. Matthew, A. Vahid, G. Brian, P. S. Johanna, D. Lawence, D. Ananth, F. B. Paul and A. K. Brian, *J. Am. Chem. Soc.*, 2008, **130**, 16770.
12 J. L. Shay, B. Tell, L. M. Schiavon, H. M. Kasper and F. Thiel, *Phys. Rev. B: Solid State*, 1974, **9**, 1719.
13 G. X. Zhu and Z. Xu, *J. Am. Chem. Soc.*, 2011, **133**, 148.
14 R. Bose, G. Manna, S. Jana and N. Pradhan, *Chem. Commun.*, 2014, **50**, 3074.
15 D. Uttiya, K. S. Sudip and J. P. Amlan, *Sol. Energ. Mater. Sol. Cells*, 2014, **124**, 79.
16 M. Venkatesh, N. Venkatram, S. M. Pradipta, V. Suresh and J. Wei, *J. Appl. Phys.*, 2013, **113**, 123107.
17 M. J. Deng, S. L. Shen, X. W. Wang, Y. J. Zhang, H. R. Xu, T. Zhang and Q. B. Wang, *Cryst. Eng. Commun.*, 2013, **15**, 6443.
18 S. K. Saha, A. Guchhait and A. J. Pal, *Phy. Chem. Chem. Phys.*, 2014, **16**, 4193.
19 Z. S. Luo, H. Zhang, J. Huang and X. H. Zhong, *Jounal of Colloid and Interface Science*, 2012, **1**, 27.
20 M. L. Dai, S. J. Oqawa, T. Kameyama, K. Okazaki, A. Kudo, S. Kuwabata, Y. Tsuboi and T. Torimoto, *J. Mater. Chem.*, 2012, **22**, 12851.
21 T. Torimoto, T. Adachi, K. Okazaki, M. Sakuraoka, T. Shibayama, B. Ohtani, A.Kudo, S. Kuwabata, *J. Am. Chem. Soc.*, 2007, **129**, 12388.
22 B. D. Mao, C. H. Chuang, J. W. Wang and C. Bruda, *J. Phys. Chem. C*, 2011, **15**, 8945.
23 H. Z. Zhong, Z. Bai and B. S. Zou, *J. Phys. Chem. L*, 2012, **3**, 3167.
24 Z. Aissa, T. Ben Nasrallah, M. Amlouk, J. C. Bernede and S. Belgacem, *Sol. Energ. Mater. Sol. Cells*, 2006, **5**, 1136.
25 Q. Cheng, X. H. Peng and Candace K. Chan, *ChemSusChem*, 2013, **6**, 102.
26 Y. Akaki, S. Kurihara, M. Shirahama, K. Tsurugida, S. Seto, T. Kakeno and K. Yoshino, *J. Phys. Chem. Solid*, 2005, **66**, 1858.
27 C. H. Wang, K. W. Cheng and C. J. Tseng, *Sol. Energ. Mater. Sol. Cells*, 2011, 9**5**, 453.
28 H. Lin, C. C. Wu, C. H. Lai and T. C. Lee, *Chem. Mater*, 2008, **20**, 4475.
29 B. R. Sankapal, E. Goncalves, A. Ennaoui and M. C. Lux-Steiner, *Thin Solid Films*, 2004, **451**, 128.
30 S. J. Peng, S. Y. Zhang, S. G. Mhaisalkar and S. Ramakrishna, *Phys. Chem. Chem. Phys.*, 2012, **14**, 8523.
31 J. H. Han, Z. F. Liu, K. Guo, J. Ya, Y. F. Zhao, X. Zhang, T. T. Hong and J. Q. Liu, *ACS Appl. Mater. Interfaces*, 2014, **6**, 17119.
32 K. P. Kadlag, P. Patil, M. J. Rao, S. Datta and A. Nag, *Cryst. Eng. Commun.*, 2014, **16**, 3605.
33 T. Sasamura, K. I. Okazaki, A. Kudo, S. Kuwabata and T. Torimoto, *RSC Adv.*, 2012, **2**, 552.
34 T. L. Li, Y. L. Lee and H. S. Teng, *Energy Environ. Sci.*, 2012, **5**, 5315.
35 (34) P. K. Santra, P. V. Nair, K. G. Thomas and P. V. Kamat, *J. Phys. Chem. Lett.*, 2013, **4**, 722.
36 S. Ruhle, S. Yahav, S. Greenwald and A. Zaban, *J. Phys. Chem. C*, 2012, **116**, 17473.
37 P. K. Santra and P. V. Kamat, *J. Am. Chem. Soc.*, 2012, **134**, 2508.
38 S. Giménez, A. L. Rogach, A. A. Lutich, D. Gross, A. Poeschl, A. S. Susha, I. Mora-Seró, T. Lana-Villarreal and J. Bisquert, *J. Appl. Phys.*, 2011, **110**, 014314.
39 J. Y. Chang, J. M. Lin, L. F. Su and C. F. Chang, *ACS Appl. Mater. Interfaces*, 2013, **5**, 8740.
40 X. Hu, Q. X. Zhang, X. M. Huang, D. M. Li, Y. H. Luo, Y. H. Luo and Q. B. Meng, *J. Mater. Chem.*, 2011, **21**, 15903.
41 Y. Q. Wang, Y. C. Rui, Q. H. Zhang, Y. G. Li, H. Z. Wang, *ACS Appl. Mater. Interfaces*, 2013, **5**, 11858.
42 M. A. Franzman and R. L. Brutchey, *Chem. Mater.*, 2009, **21**, 1790.
43 W. M. Qiu, M. S. Xu, X. Yang, F. Chen, Y. X. Nan, J. L. Zhang, H. Iwai and H. Z. Chen, J. Mater. Chem., 2011, **21**, 13327.
44 A. Yella, H. W. Lee, H. N. Tsao, C. Y. Yi, A. K. Chandiran, M. K. Nazeeruddin, E. W. G. Diau, C. Y. Yeh, S. M. Zakeeruddin and M. Grätzel, *Science*, 2011, **334**, 629.
45 T. Bessho, S. M. Zakeeruddin, C. Yeh, E. W. G. Diau and M. Grätzel, *Angew. Chem. Int. Edit.*, 2010, **49**, 6646.
46 A. Tubtimtae, K. L. Wu, H. Y. Tung, M. W. Lee and G. J. Wang, *Electrochem. Commun.*, 2010, **12**, 1158.
47 Z. L. Liu, K. B. Tang, D. Wang, L. L. Wang and Q. Y. Hao, *Nanoscale*, 2013, **5**, 1570.
48 S. M. Yang, C. H. Huang, J. Zhai, Z. S. Wang and L. Jiang, *J. Mater. Chem.*, 2002, **12**, 1459.
49 G. Hodes, J. Manassen and D. Cahen, *Electrochem. Soc.,* 1980, **127**, 544.
50 I. Robel, V. Subramanian, M. Kuno and P. V. Kamat, *J. Am. Chem. Soc.*, 2006, **128**, 2385.
51 Y. W. Tang, X. Y. Hu, M. J. Chen, L. J. Luo, B. H. Li and L. Z. Zhang, *Electrochim. Acta*, 2009, **54**, 2742.
52 H. Wang, Y. S. Bai, H. Zhang, Z. H. Zhang, J. H. Li and L. Guo, *J. Phys. Chem. C*, 2010, **114**, 16451.
53 H. Chen, W. Y. Fu, H. B. Yang, P. Sun, Y. Y. Zhang, L. R. Wang, W. Y. Zhao, X. M. Zhou, H. Zhao, Q. Jing, X. F. Qi and Y. X. Li, *Electrochim. Acta*, 2010, **56**, 919.